Catalysis Science & Technology

Accepted Manuscript

ROYAL SOCIETY OF CHEMISTRY

www.rsc.org/catalysis

Adsorption and transformations of ethene on hydrogenated rhodium clusters in faujasite-type zeolite. A computational study†

Velina K. Markova,[a] Georgi N. Vayssilov,[a]* Alexander Genest,[b] and Notker Rösch[b,c]*

[a] *Faculty of Chemistry and Pharmacy, University of Sofia, Blvd. J. Baucher 1, 1126 Sofia, Bulgaria. Email: gnv@chem.uni-sofia.bg*
[b] *Institute of High Performance Computing, Agency for Science, Technology and Research, 1 Fusionopolis Way, #16-16 Connexis, Singapore 138632, Singapore*
[c] *Department Chemie and Catalysis Research Center, Technische Universität München, 85747 Garching, Germany. Email: roesch@mytum.de*

Abstract

Regarding the heterogeneous catalytic hydrogenation of ethene on small rhodium clusters, anchored in faujasite, we studied computationally intermediates C_2H_x (x = 2–5) on zeolite-supported Rh_3 and Rh_4 clusters with pre-loaded hydrogen. According to calculated Gibbs free energies, at temperatures and hydrogen pressure values representing pertinent experiments, the favored stable species on hydrogen-loaded Rh_3 is ethylidyne which apparently prevents further hydrogenation due to its strong $CH_3\text{-}C\equiv Rh_n$ interaction. In contrast, on bare and hydrogenated Rh_4 clusters, partially hydrogenated C_2H_5 species, locally stable intermediates, are among the most stable adsorption complexes examined. These "pseudo-ethyl" C_2H_5 ligands exhibit a very specific structure, where both carbon atoms and a hydrogen atom of the organic moiety interact with the apical Rh center of Rh_4; previously such ligand structures have been identified only computationally as transition states in homogeneous catalysis of ethene hydrogenation. According to our analysis based on thermodynamic phase diagrams, one is lead to conclude that only Rh clusters of such specific topology may be appropriate for the catalytic hydrogenation of ethene, in contrast to zeolite-supported Rh_3 clusters. Suggestions are made for further probing this size-specific catalytic activity of Rh clusters.

† Electronic Supplementary Information (ESI) available: Figures showing the structures of all complexes modeled, variation of the charges, interatomic distances, and phase diagram of the dominant k values. Tables with charges and vibrational frequencies of the complexes. Comments on the structures, charges, and vibrational frequencies. Description of the thermodynamic model. Cartesian coordinates of the complexes.

1. Introduction

Small supported clusters of noble transition metals are particularly interesting for catalysis since they combine the high catalytic activity of those metals in various catalytic processes with low amount of the expensive precious metal. Such clusters, however, may have a very different catalytic behavior than the corresponding metal surfaces or mononuclear metal species.[1-3] Other properties of metal containing catalysts can also play a role in the catalytic activity and selectivity, e.g. the size of the clusters and the nature of the support, as recently shown for Rh species.[4] From extended x-ray absorption fine structure (EXAFS) data and infrared (IR) spectroscopy it was concluded that in the presence of small Rh clusters, e.g., Rh_3, Rh_4, or Rh_6,[4,5] supported on HY zeolite (with faujasite structure) and in the presence of H_2 the dominant reaction of a C=C bond is hydrogenation, in contrast to mononuclear ionic Rh species that catalyze the dimerization of olefins.[4] That catalytic system is particularly interesting as the nuclearity of the metal species and the reaction products crucially depend on the ethene-to-hydrogen ratio in the feed. Using time-resolved IR spectroscopy, Gates et al. suggested[6] various intermediates during the hydrogenation reaction, e.g., ethyl and ethylidyne. Other experiments, using temperature-programmed static secondary ion mass spectrometry, predicted vinyl to exist on a Rh(111) surface upon that interacts ethene.[7]

While various theoretical studies of ethene adsorption on rhodium surfaces have been reported,[8-10] the interaction of ethene or related surface intermediates with small rhodium clusters still remains computationally unexplored. Such studies are particularly important for the experiment in view of the available experimental studies for ethene hydrogenation on such clusters, anchored in faujasite.[4,5] As experiments have been performed for different ethene-to-hydrogen ratios in the reaction feed, a consistent computational model requires accounting for the presence of hydrogen on the metal clusters. Therefore, we carried out a model study of potential intermediates that may be formed upon adsorption of ethene on small Rh_n clusters ($n = 3, 4$), supported on zeolites with a faujasite-type framework and carrying variable amounts of pre-adsorbed hydrogen ligands. Such model studies accounting for the presence of co-adsorbed hydrogen are rather rare for small supported metal clusters[11] and completely missing for small rhodium clusters. Experiments suggest that the reaction is complicated. Therefore, we first studied the hydrogenation of zeolite-supported rhodium clusters[12] and modeled the thermodynamics of hydrogenated clusters for large ranges of temperature and H_2 pressure. In the present work we report the influence of the hydrogen coverage and the size of the rhodium cluster on the relative stability of various organic species.

Similar to previous studies of ethene-derived species on metal clusters or surfaces,[13-15] we address here the structure and the stability of different intermediates that may appear from hydrogenation (ethyl), dehydrogenation (ethylidyne, vinyl, vinylidene) or isomerization (ethylidene) of ethene-derived species when ethene adsorbs on small hydrogenated rhodium clusters. The results of the calculations allowed us to construct a thermodynamic model for both Rh_3 and Rh_4 clusters that revealed the dominant organic species on each size of the clusters depending on the temperature and the hydrogen pressure. We also analyzed the charges of the organic adsorbates and metal moiety; see Electronic Supplementary Information (ESI). Where appropriate, we compared calculated vibrational frequencies of the most stable species to experimental values, see ESI.

2. Computational details

2.1. Zeolite models

The models used for the calculations were inspired by our previous work.[12] We again represented a faujasite-type zeolite framework, periodic in three dimensions, by a rhombic unit cell (with the parameters a = b = c = 17.34 Å and α = β = γ = 60°) containing 48 crystallographically equivalent T atoms, where one of them is Al, and the other 47 are Si atoms. The shape and the volume of the zeolite system have been relaxed without adsorbate. The negative charge of the zeolite framework around the Al site in the pristine structure is compensated by a proton forming a bridging hydroxyl group. After deposition of the bare rhodium cluster in the zeolite cavity, this proton is transferred to the metal cluster via reverse hydrogen spillover which may be also viewed as an electron-coupled proton transfer. According to our earlier work,[12] the most preferable adsorption site for the bare and hydrogenated H_mRh_n clusters (n = 3, 4) in the supercage of the faujasite structure is near the Al center at the junction of three four-member rings (4R) of the zeolite framework. Therefore here we selected this adsorption site for the complexes of organic species at supported H_mRh_n clusters.[12] These model clusters were formed by (*i*) formal reverse hydrogen spillover from zeolite hydroxyl group onto the (hydrogenated) Rh_3 or Rh_4 clusters and (*ii*) by subsequent (dissociative) addition of H_2 molecules on the metal cluster, three H_2 molecules for Rh_3 and four molecules for Rh_4. Recall that our previous calculations have shown reverse hydrogen onto the small Rh clusters to be energetically favorable.[12,16,17]

Regarding the organic adsorbates on these hydrogenated Rh clusters, we examined the adsorption of ethene, followed adsorption complexes of organic intermediates that formally result by hydrogenation (e.g., forming ethyl from ethene) or dehydrogenation of intermediates (e.g., vynil, vynilidene, ethylidyne) with less hydrogen content. We denote the adsorption complexes as $C_2H_x/H_{k-x}Rh_n$ where k = x+m is the total number of hydrogen atoms in the system and m is the number of hydrogen ligands on the metal cluster, derived from adsorbed H_2 molecules, reverse H spillover from the bridging OH group, or the organic ligand.

2.2. Electronic structure method

All calculations were carried out using the Vienna ab initio simulation package (VASP),[18,19] invoking the exchange-correlation functional in the form of the generalized gradient approximation, specifically the functional suggested by Perdew, Burke, and Ernzerhof (PBE).[20] We sampled the Brillouin zone at the Γ point only as the unit cell employed in the calculations is quite large. The ion–electron interactions were represented by the projector-augmented wave method (PAW).[21,22] The plane-wave representation of the valence wave functions was characterized by an energy cutoff of 400 eV. The calculations with tetra-atomic rhodium clusters were carried out in spin-restricted fashion whereas the calculations for the three-atomic cluster are done in spin-polarized fashion in view of the odd number of electrons in the hydrogenated cluster models (see Fig. 1). Self-consistency was considered to be reached when the total energy changed less than 10^{-6} eV between subsequent cycles; the geometry optimization was stopped when all forces on ions were less than 0.02 eV/Å. van der Waals interactions were taken into account by the DFT-D2 method.[23]

We verified all local minimum structures by a partial normal mode analysis that included the atoms of the adsorption complexes $C_2H_x/H_{k-x}Rh_n$ and all atoms of the three four-membered rings of the zeolite framework that make up the immediate coordination sphere of the metal moiety; the remaining part of the zeolite framework was kept fixed. The vibrational frequencies were calculated in the harmonic approximation by diagonalizing the mass-weighted Hessian matrix. The matrix elements were constructed from finite differences of the first-order derivatives of the total energy, by shifting each of the ions from the optimized structure in all Cartesian directions. None of the reported structures showed an imaginary vibrational frequency. Atomic charges of the complexes $C_2H_x/H_{k-x}Rh_n$ were calculated using a Bader-type analysis.[24]

We evaluated the stability of the species $C_2H_x/H_{k-x}Rh_n$ by relative energies, ΔE, Gibbs free energies, ΔG, and binding energies of ethene, BE_{eth}, or hydrogen, BE_H, defined as follows:

- relative stability ΔE with respect to the most stable organic species of the same composition, i.e. the same number k of H atoms;
- Gibbs free energy ΔG calculated with respect to the π-bonded ethene adsorption complex C_2H_4/HRh_n, with the lowest number of H (k = 5, which includes x = 4 H atoms of the organic ligand, and one H transferred from the bridging OH group from the zeolite):

  $$\Delta G(C_2H_x/H_{k-x}Rh_n) = G(C_2H_x/H_{k-x}Rh_n) - G(C_2H_4/HRh_n) - \tfrac{1}{2}(k-5)\, G(H_2);$$

- binding energy of ethene BE_{eth} of each ethene-containing structure $C_2H_4/H_{k-4}Rh_n$ with respect to ethene in the gas phase and the adsorption complex, $H_{k-4}Rh_n$, with the same number and type of coordination of H ligands. The energy of the latter structure was obtained by a single-point calculation after removal of the ethene molecule from the complex $C_2H_4/H_{k\text{-}4}Rh_n$, but without re-optimization to preserve the configuration of the H ligands:

$$BE_{eth} = E(C_2H_4/H_{k\text{-}4}Rh_n) - E(H_{k\text{-}4}Rh_n) - E(C_2H_4)$$

E is the total energy of the system indicated.

- average binding energy BE_H of H atoms of $C_2H_x/H_{k\text{-}x}Rh_n$, calculated with respect to H_2 in the gas phase and the most stable structure and lowest hydrogen loading (k = 5) with the same intermediate $C_2H_x/H_{5\text{-}x}Rh_n$:

$$BE_H = [E(C_2H_x/H_{k\text{-}x}Rh_n) - E(C_2H_x/H_{5\text{-}x}Rh_n) - ½(k–x–1)\ E(H_2)\ ]/(k\text{-}x\text{-}1)$$

For all these definitions, more negative values correspond to more stable structures.

2.3. Thermodynamic model

We used the relative Gibbs free energies of the complexes $C_2H_x/H_{k\text{-}x}Rh_n$ to construct a thermodynamic model for the hydrogen coverage as function of the temperature and the H_2 pressure. The relative Gibbs free energy, $\Delta G(C_2H_x/H_{k\text{-}x}Rh_n)$, of a structure $C_2H_x/H_{k\text{-}x}Rh_n$ (n = 3, 4) is defined via its formal formation from the system, C_2H_4/HRh_n, with adsorbed ethene and the lowest hydrogen coverage, supported in the zeolite, after adsorption of ½(k–5) H_2 molecules from the gas phase:

$$C_2H_4/HRh_n + ½(k–5)\ H_2 \rightarrow C_2H_x/H_{k\text{-}x}Rh_n$$

$$\Delta G(C_2H_x/H_{k\text{-}x}Rh_n) = \Delta H(C_2H_x/H_{k\text{-}x}Rh_n) - T\Delta S(C_2H_x/H_{k\text{-}x}Rh_n)$$

Here $\Delta H(C_2H_x/H_{k\text{-}x}Rh_n)$ is the corresponding change in enthalpy (including the electronic energy E and the zero-point energy correction); $\Delta S(C_2H_x/H_{k\text{-}x}Rh_n)$ is the change in entropy, determined in standard fashion from the partition functions q of the corresponding clusters and the appropriate number of H_2 molecules in the gas phase.[25] The free rotation and the free translation were taken into account only for the H_2 molecules, but not for the adsorption complexes systems $C_2H_x/H_{k\text{-}x}Rh_n$ and C_2H_4/HRh_n because their rotational and translational degrees freedom are restricted by the interaction of the rhodium atoms with the zeolite framework. When calculating the vibrational entropy contribution, we accounted only for atoms of the adsorption complexes $C_2H_x/H_{k\text{-}x}Rh_n$ and the atoms of the three four-member rings at the adsorption site.

The molar fractions, α_m, of all adsorption complexes at specific temperature T and hydrogen pressure $P(H_2)$ were determined by the equilibrium constant, $K(C_2H_x/H_{k\text{-}x}Rh_n)$ which, in turn, were obtained from the relative Gibbs free energy of the species;[25,26] for details; see Section 1 of the ESI. In this statistical thermodynamic approach, small changes in the ΔG values will notably change the phase diagrams.

3. Results

First we will discuss the structural characteristics of the adsorbed intermediates, C_2H_x, on hydrogenated rhodium clusters, $H_{k-x}Rh_n$, focusing on the coordination type, the influence of the organic species on the structure of the metal cluster and its interaction with the support. Then we will compare the relative stability of the species for a certain amount k of hydrogen to identify the most stable organic adsorbate among this group of adsorption systems. The characteristic structural and energetic parameters of ethene adsorbates and all intermediates (derived from ethene) are shown in Tables 1 and 2 for the clusters Rh_3 and Rh_4, respectively. Figure 1 shows the optimized structures of all types of organic species in the complexes of Rh_3 and Rh_4 clusters for the lowest number of H atoms in the system, k = 5. Selected structures with higher hydrogen loading are shown in Figures 2 and 3. In Section 2 of the ESI, we provide a more detailed discussion of the complexes as well as sketches of all structures reported in Tables 1 and 2; see Figs. S1 to S4 of the ESI. In Figure S5 of the ESI we show the location of the complexes in the faujasite channel on the example of the complex C_2H_5/H_8Rh_4.

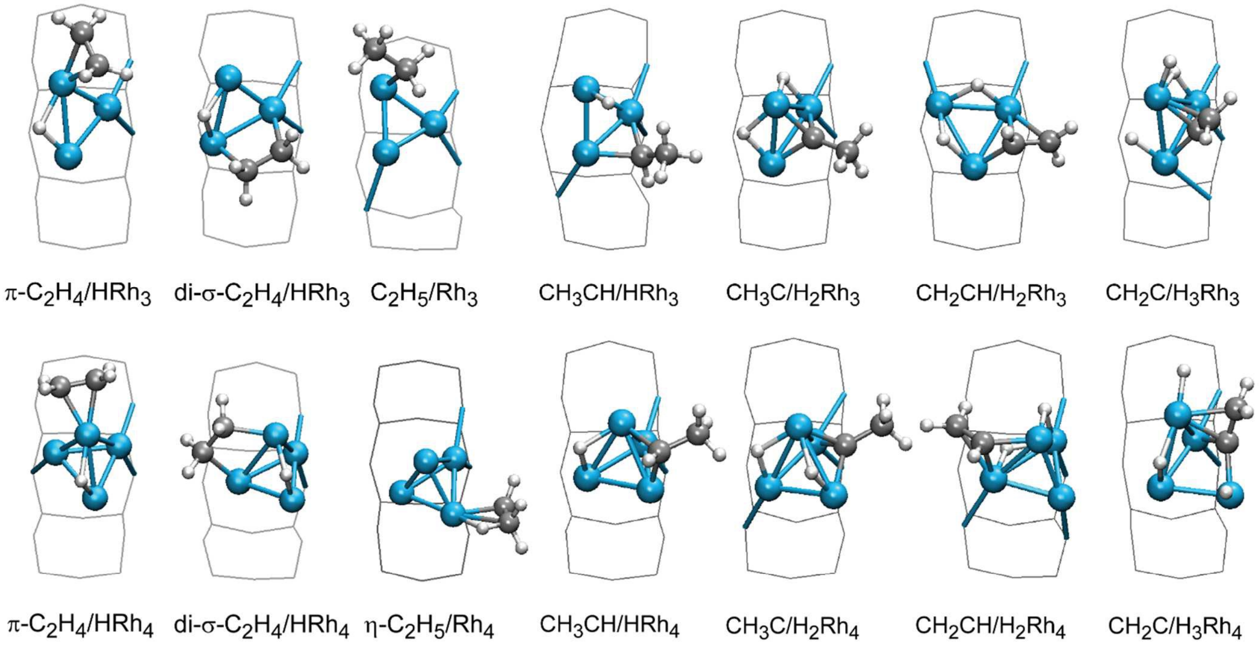

Figure 1. Optimized structures of the complexes of the clusters Rh_3 (upper row) and Rh_4 (lower row) with the lowest numbers, k = 5, of H atoms in the system. Organic ligands from left to right: π-bonded ethene, di-σ-bonded ethene, ethyl, ethylidene, ethylidyne, vinyl, vinylidene.

3.1. Structure of the organic species and rhodium clusters

3.1.1. Structure and binding of the organic species

Rh_3 cluster. For the clusters H_nRh_3 we modeled two coordination modes of ethene, di-σ- and π-bonded (Figs. 1, 2). In the first case, each C atom binds to a separate Rh atom, while the two C atoms of π-bonded ethene interact with a single Rh center. At the cluster Rh_3 ethylidene prefers to coordinate in a bridging fashion as the C atom of the CH moiety interacts with two Rh centers (Fig. 1). The intermediate ethylidyne coordinates in three-fold fashion to all centers of Rh_3 (Figs. 1, 2). Similar to ethylidene, the CH moiety of vinyl coordinates to a Rh-Rh bond of the cluster; the carbon center of the CH_2 moiety is also bound to one of those metal atoms. This coordination of vinyl differs from that determined on a Rh(111) surface[8] or on small transition metal clusters[15,27] where the intermediate interacts with three metal centers and the C-C bond is parallel to the surface, defined by those centers. In our model system with the zeolite-supported Rh_3 cluster, the latter coordination mode was calculated to have a lower stability, likely due to the small size of the metal species.

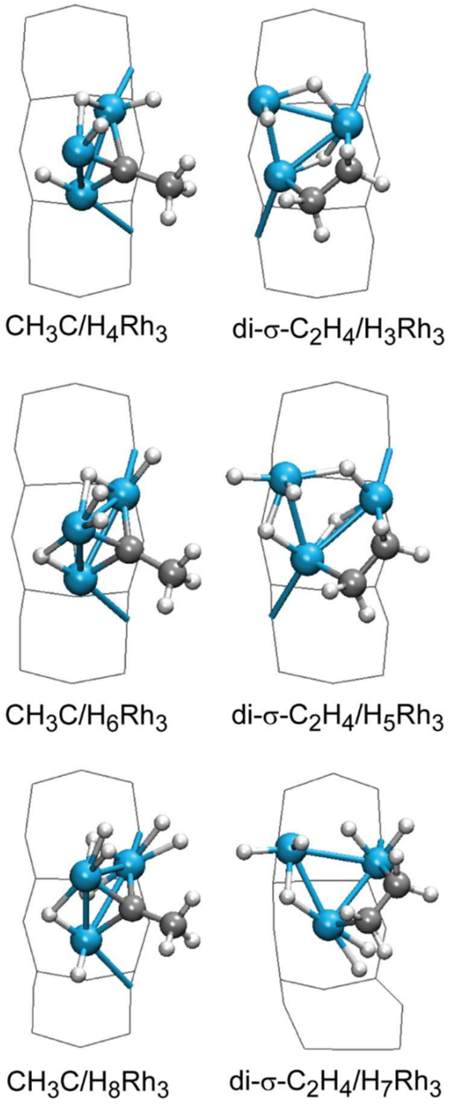
CH_3C/H_4Rh_3 di-σ-C_2H_4/H_3Rh_3

CH_3C/H_6Rh_3 di-σ-C_2H_4/H_5Rh_3

CH_3C/H_8Rh_3 di-σ-C_2H_4/H_7Rh_3

Figure 2. Optimized structures of selected $C_2H_x/H_{k-x}Rh_3$ complexes with $k > 0$. The most stable ethylidyne species on this metal cluster (left-hand column) and the most stable adsorption mode of di-σ-bonded ethene (right-hand column).

Table 1. Energy (kJ/mol) and structure (pm) characteristics of organic species on bare and hydrogenated zeolite-supported Rh_3 clusters, calculated for $C_2H_x/H_{k-x}Rh_3$ models.

	ΔE	BE_H	BE_{eth}	Rh-Al	<Rh-O>/n[a]	<Rh-Rh>	C-C	Rh-C
di-σ-Ethene								
di-σ-C_2H_4/HRh_3	72.5		-231.6	289	231/2	247	148	203, 208
di-σ-C_2H_4/H_3Rh_3	0.0	-51.3	-260.6	327	235/3	258	149	203, 205
di-σ-C_2H_4/H_5Rh_3	35.5	-38.9	-271.1	325	231/2	274	148	204, 207
di-σ-C_2H_4/H_7Rh_3	103.6	-29.5	-232.4	346	230/2	272	149	205, 211
π-Ethene								
π-C_2H_4/HRh_3	114.5		-199.1	287	226/2	247	142	211, 213
π-C_2H_4/H_3Rh_3	12.5	-66.1	-205.2	300	220/1	252	140	212, 213
π-C_2H_4/H_5Rh_3	76.3	-39.2	-160.9	308	234/1	272	140	218, 218
π-C_2H_4/H_7Rh_3	74.7	-41.3	-135.7	297	232/3	272	138	227, 228
Ethyl								
C_2H_5/HRh_3	162.8			283	230/3	240	153	203
C_2H_5/H_2Rh_3	59.0	-67.0		289	233/3	248	151	205
C_2H_5/H_4Rh_3	14.6	-66.7		288	230/2	261	152	202
C_2H_5/H_6Rh_3	65.3	-50.9		290	234/3	272	151	206
Ethylidene								
CH_3CH/HRh_3	102.6			283	232/3	246	150	197, 203
CH_3CH/H_3Rh_3	2.7	-65.0		289	234/3	260	150	199, 200
CH_3CH/H_5Rh_3	39.0	-45.6		293	232/2	271	151	199, 203
CH_3CH/H_7Rh_3	81.1	-38.3		342	236/2	267	150	200, 200
Vinyl								
CH_2CH/H_2Rh_3	105.0			298	227/1	254	142	197, 205, 218
CH_2CH/H_4Rh_3	33.1	-51.0		300	218/1	270	141	196, 206, 214
CH_2CH/H_6Rh_3	43.2	-45.1		297	215/1	287[b]	140	194, 216, 216
CH_2CH/H_8Rh_3	60.6	-42.1		294	226/2	285	140	196, 209, 219
Ethylidyne								
CH_3C/H_2Rh_3	0.0			288	226/2	260	149	194, 195, 193
CH_3C/H_4Rh_3	5.2	-12.5		333	228/2	268	149	191, 193, 204
CH_3C/H_6Rh_3	0.0	-29.7		334	230/2	270	150	195, 193, 199
CH_3C/H_8Rh_3	0.0	-34.7		324	230/2	270	150	192, 196, 199
Vinylidene								
CH_2C/H_3Rh_3	74.9			290	231/3	271	142	191, 194, 201, 215

[a] Average value of Rh-O distances less than 240 pm, n is the number of such contacts. [b] Average Rh-Rh distances calculated for nearest-neighbor distances of less than 300 pm.

With vinylidene as ligand, the adsorption complex of Rh_3 is stable only with lowest number of H ligands, CH_2C/H_3Rh_3, where one C atom of vinylidene coordinates in three-fold fashion to the metal cluster and the CH_2 fragment forms a Rh-C bond. At higher H loading the Rh-Rh distances increase strongly to more than 300 pm, resulting in the decay of the metal cluster. For intermediates as ethyl, on-top coordination at a Rh center was determined most favorable, irrespective of the H loading of the Rh_3 cluster. The CH_3 group of ethyl does not interact with the rhodium cluster.

The C-C distance in the species di-σ-bonded ethene, ethyl, ethylidene, and ethylidyne is in the range 148–153 pm, corresponding to a C-C single bond close to 152 pm, calculated for the isolated ethane molecule. The C-C distances in the other species, 138–142 pm, suggest an elongated double C=C bond compared to the value obtained for an isolated ethene molecule, 133 pm.

***Rh_4* cluster.** The coordination modes of π- and di-σ-bonded ethene on the supported Rh_4 cluster as well as those of the intermediates ethylidene and ethylidyne (Figs. 1, 3) are similar to the structures of the analogous adsorption complexes of the Rh_3 cluster. Related structures of corresponding adsorption complexes differ mainly in the Rh-C distances. For ethylidyne also Rh-Rh distances are affected, namely for the complexes $CH_3C/H_{k-3}Rh_4$ with more than one H ligand. Ethylidyne as ligand induces a change of the tetrahedral shape of the cluster as one of the Rh-Rh distances (involving a Rh atom interacting with the organic ligand) becomes longer than 300 pm.

Also the intermediates vinyl and vinylidene coordinate to Rh_4 essentially in the same way as to Rh_3. For high H loading with 6, 8, and 10 H ligands on the Rh_4 moiety, we determined two of the Rh-Rh distances of the vinylidene adsorption complex longer than 300 pm.

The coordination of the most stable ethyl species, calculated on a H_nRh_4 cluster, differs from that of a standard ethyl species which binds on-top of a Rh center, e.g. in the adsorption complex of Rh_3. Indeed, in the supported H_nRh_4 clusters, n = 0–8, the CH_3 group forms two bonds to the metal moiety, via the carbon and one hydrogen center. To distinguish this specific bonding, we refer to these structures as *pseudo ethyl* and denote them as η-$C_2H_5/H_{k-5}Rh_4$ (Figures 1, 3; Table 2). This bonding Rh-H distance is 195 pm in η-C_2H_5/Rh_4 and reduces to 178–180 pm for higher H loading of the cluster. As such distances are similar to those calculated for bridge coordinated H ligands adsorbed on rhodium clusters, one indeed can consider these contacts as bonds.[12] The C-H distances of the H atoms involved in this type of bonding, 116 pm for η-C_2H_5/Rh_4 and 122 pm at cluster of higher H loading, are by 11 pm longer than the regular C-H distance in a methyl group. In these complexes the two C atoms interact with the same Rh center as the H atoms of the CH_3 fragment. The Rh-C distance of the CH_2 fragment is 204–207 pm, while the Rh-C contact involving the methyl group is notably longer, 228–239 pm. The literature does not seem to provide an analogue for this coordination mode of an ethyl moiety to a metal moiety, likely because its formation may require an apical metal atom of a larger metal moiety, here of Rh_4. However, similar coordination modes of CH_3CH_2 species are typical for transition state (TS) structures of hydrogenation reactions involving π-bonded ethene.[8,13,14]

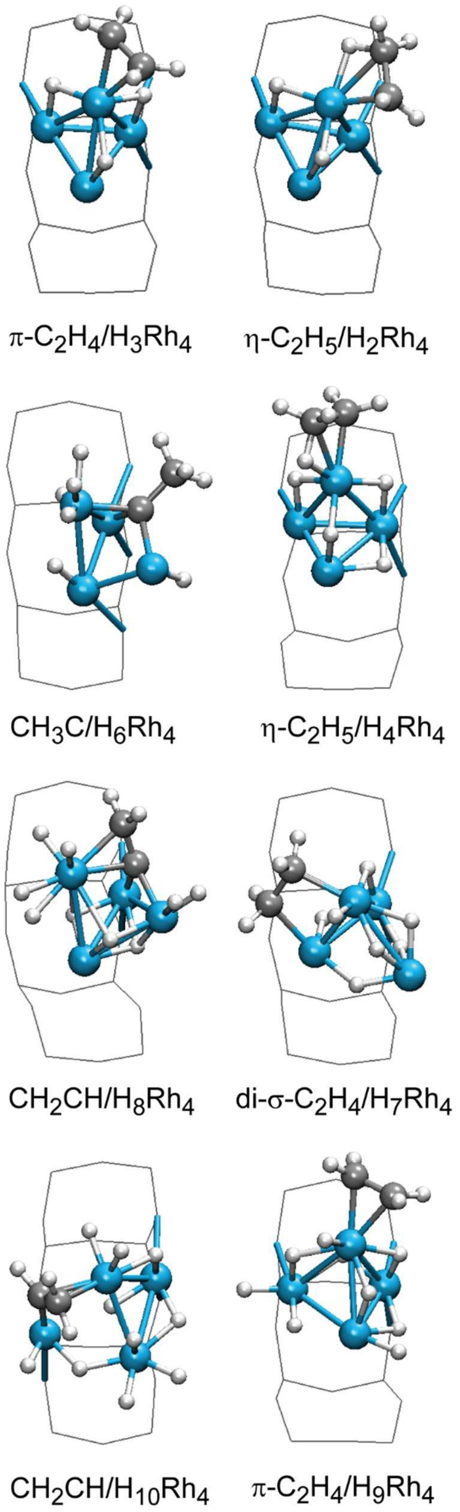

π-C_2H_4/H_3Rh_4 η-C_2H_5/H_2Rh_4

CH_3C/H_6Rh_4 η-C_2H_5/H_4Rh_4

CH_2CH/H_8Rh_4 di-σ-C_2H_4/H_7Rh_4

$CH_2CH/H_{10}Rh_4$ π-C_2H_4/H_9Rh_4

Figure 3. Optimized structures of selected $C_2H_x/H_{k\text{-}x}Rh_4$ complexes for $k > 0$: the most stable complexes at different conditions according to the ΔG values (π-bonded ethene, pseudo ethyl and ethylidyne) as well as species with a broken Rh-Rh bond (di-σ-bonded ethene and vinyl).

Table 2. Energy (kJ/mol) and structure (pm) characteristics of organic species on bare and hydrogenated zeolite-supported Rh_4 clusters, calculated for $C_2H_x/H_{k-x}Rh_4$ models.

	ΔE	BE_H	BE_{eth}	Rh-Al	<Rh-O>/n[a]	<Rh-Rh>	C-C	Rh-C	Rh-H[b]	C-H[b]
di-σ-Ethene										
di-σ-C_2H_4/HRh_4	51.3		-216.5	289	225/2	253	147	202, 203		
di-σ-C_2H_4/H_3Rh_4	4.6	-69.7	-218.5	294	225/2	253	148	209, 210		
di-σ-C_2H_4/H_5Rh_4	52.8	-44.6	-193.6	293	228/2	264	147	213, 211		
di-σ-C_2H_4/H_7Rh_4	49.7	-40.6	-197.0	291	230/3	270^c	146	212, 214		
di-σ-C_2H_4/H_9Rh_4	54.7	-40.9	-250.2	293	224/2	274^c	148	210, 211		
π-Ethene										
π-C_2H_4/HRh_4	0.0		-203.1	287	227/2	250	141	211, 213		
π-C_2H_4/H_3Rh_4	10.6	-41.0	-194.3	290	227/2	257	142	214, 214		
π-C_2H_4/H_5Rh_4	21.1	-39.7	-194.5	289	229/3	266	141	215, 215		
π-C_2H_4/H_7Rh_4	5.7	-39.4	-210.4	293	225/2	265	142	214, 214		
π-C_2H_4/H_9Rh_4	0.0	-41.3	-213.7	290	227/3	279	141	214, 216		
Ethyl										
η-CH_3CH_2/Rh_4	102.5			292	228/2	247	151	204, 239	195	116
η-CH_3CH_2/H_2Rh_4	0.0	-97.6		288	228/2	253	148	205, 228	179	122
η-CH_3CH_2/H_4Rh_4	0.0	-70.6		294	226/2	264	148	206, 231	180	121
η-CH_3CH_2/H_6Rh_4	0.0	-57.4		296	226/2	270	148	207, 230	178	122
η-CH_3CH_2/H_8Rh_4	0.5	-54.1		290	228/3	281	148	206, 229	178	122
Ethylidene										
CH_3CH/HRh_4	63.7			292	225/2	254	152	197 ,199		
CH_3CH/H_3Rh_4	62.9	-46.7		295	225/2	261	152	196, 199		
CH_3CH/H_5Rh_4	69.7	-43.4		301	232/3	269	150	196, 205		
CH_3CH/H_7Rh_4	44.5	-43.5		296	230/3	271	151	204, 195		
CH_3CH/H_9Rh_4	74.2	-40.0		299	225/2	271	151	197, 198		
Vinyl										
CH_2CH/H_2Rh_4	63.1			292	231/4	257	139	202, 199, 237		
CH_2CH/H_4Rh_4	59.4	-48.2		295	230/3	262	142	200, 200, 215		
CH_2CH/H_6Rh_4	37.9	-51.2		293	222/2	272	141	195, 205, 219		
CH_2CH/H_8Rh_4	10.2	-49.1		294	223/2	287	141	194, 206, 218		
$CH_2CH/H_{10}Rh_4$	29.9	-45.5		289	228/3	282^c	141	198, 209, 218		
Ethylidyne										
CH_3C/H_2Rh_4	54.3			291	233/3	270	151	193, 199, 192		
CH_3C/H_4Rh_4	77.7	-34.7		286	232/3	264^c	150	196, 196, 197		
CH_3C/H_6Rh_4	16.7	-54.4		288	230/3	267^c	150	198, 201, 192		
CH_3C/H_8Rh_4	75.4	-36.8		292	232/3	269^c	150	194, 198, 201		
$CH_3C/H_{10}Rh_4$	64.9	-40.0		292	232/3	268^c	150	196, 198, 200		
Vinylidene										
CH_2C/H_3Rh_4	56.4			290	229/2	265^c	144	189, 195, 205, 208		
CH_2C/H_5Rh_4	97.3	-25.9		301	229/2	276	142	193, 195, 204, 209		
CH_2C/H_7Rh_4	41.8	-48.6		302	229/2	275^c	143	192, 193, 207, 210		

[a] Average value of Rh-O distances less than 240 pm, n is the number of the such contacts. [b] C and H centers of the CH_3 moiety. [c] Average Rh-Rh distances calculated for nearest-neighbor distances of less than 300 pm.

However, the C-H distances in those TS structures on (111) surfaces were calculated somewhat longer, 133 pm on Rh(111),[8] 180 pm on Pt(111),[13] and 143 pm on Pd(111).[14]. No doubt, both types of Rh-C contacts represent bonding interactions because even the longest Rh-C distance, calculated here, is by 141 pm shorter than the sum of the van der Waals radii of Rh (195 pm) and C (185 pm). Thus, the pseudo ethyl species features three bonds of an apical Rh atom to two C and one H atoms.

A normal-mode analysis of the pseudo ethyl complexes clearly showed that these species are local minima of the potential energy surface. The calculated harmonic vibrational frequencies also allow one to discriminate the pseudo ethyl species, formed on supported Rh_4, from the regular ethyl ligands of a metal moiety, e.g., those formed on supported Rh_3. The C-H symmetric and anti-symmetric stretching frequencies of the free CH_3 group of on-top coordinated ethyl species on a supported Rh_3 cluster were calculated in the range 3080–2880 cm^{-1}, while the specific stretching mode of the elongated C-H bond of a pseudo ethyl species on the Rh_4 cluster was calculated at notably lower frequencies, 2430 cm^{-1} for $k = 5$ and between 2014 cm^{-1} and 1946 cm^{-1} for complexes with $k > 5$; see Tables S3 and S4 in ESI. It seems worthwhile to search for such pseudo ethyl species using these key vibrational characteristics.

Similarly to the complexes on the Rh_3 cluster, the C-C distance in different organic species on supported Rh_4 clusters correlates with the corresponding bond order. For species with a formal single bond, di-σ-bonded ethene, pseudo ethyl, ethylidene and ethylidyne, the C-C distance is calculated in the range 148–152 pm. Species with formal double bond, e.g., π-bonded ethene, vinyl, and vinylidene, show elongated double C=C bonds, 139–144 pm. Note the slight shortening, by 3 pm, of the C-C distance in the pseudo ethyl species on Rh_4 cluster compared to the regular ethyl species on Rh_3 cluster (Tables 1, 2).

3.1.2. Changes in the metal clusters and its interaction with the support

According to EXAFS experiments[5] Rh_4 clusters are located near the Al sites in the zeolite framework with two short Rh-O distances of ~217 pm. In our previous investigation on hydrogenated zeolite-supported Rh_3 or Rh_4 clusters, we also found two Rh-O contacts with oxygen centers in the immediate vicinity of the Al center. This coordination changes for some of the complexes discussed here, due to an oversaturation of some of the Rh centers.

In agreement with our previous calculations on transition metal clusters[12,15,26,28] the average intermetallic distances increase when an organic moiety adsorbs and the hydrogen coverage increases (Tables 1, 2; Fig. S7 of the ESI). Recall the average Rh-Rh distances of supported HRh_3 and HRh_4 clusters, 242 pm and 247 pm,[12] respectively, which are notably shorter than the Rh-Rh distance in rhodium bulk, 268 pm.[29] EXAFS experiments on Rh_6

clusters supported on MgO showed[6] that adsorption of organic species also induces increased Rh-Rh distances. Our present results (Tables 1, 2; Fig. S7 of the ESI) show that the adsorption of ethene (π-bonded or di-σ-bonded) on supported HRh_3 and HRh_4 clusters induces an elongation of the average metal-metal distance by 5 pm and 3–6 pm, respectively. The coordination of additional H ligands to the metal moiety results in a further increase of the average Rh-Rh distance to 272 pm for the complex C_2H_4/H_7Rh_3 and 274–279 pm for the complex C_2H_4/H_9Rh_4.

The present model calculations show that an organic ligand can lead to a destruction of the smaller Rh_3 cluster and to a strong deformation of the Rh_4 cluster. In the complex CH_2CH/H_6Rh_3 the metal cluster is destroyed; the same holds as in Rh_3 complexes of vinylidene for $k > 5$; see Fig. S2 of the ESI.

For complexes with di-σ-bonded ethene on hydrogenated Rh_4 clusters with $k \geq 11$, two of the Rh-Rh distances elongate beyond 300 pm; see Fig. S3 of the ESI. In these structures, three Rh atoms form a Rh_3 cluster where the organic moiety is adsorbed; this adsorption complex interacts with the support via two Rh-O contacts. The forth Rh atom interacts with the other three Rh atoms trough a bridge-coordinated H ligand as the Rh-H distances are in the typical range for this type of coordination, 168–172 pm. For $k > 9$, vinylidene on Rh_4 also leads to more than one very long Rh-Rh distances, above 300 pm. For some structures ($CH_2CH/H_{10}Rh_4$, $CH_3C/H_{k-3}Rh_4$, $k = 7$–13) only one Rh-Rh distance is elongated and the tetrahedral shape of the Rh_4 cluster is changed to a “butterfly” shape; see Fig. S4 of the ESI.

3.2. Stability of various intermediates

3.2.1. Relative stability

Next, we compare the relative stability of organic adsorbates within series of complexes with the same composition, i.e., the same total number k of H atoms in the system, using ΔE values and Gibbs free energies of the structures studied; see Section 2.2.

Rh_3. According to the ΔE values the most stable species for most of the complexes is ethylidyne. Only for $k = 7$ the complex with di-σ-bonded ethene is by 5 kJ/mol more stable than that of ethylidyne (Table 1). Comparing the stability of the initial adsorption complexes of ethene, the di-σ-bonded configuration is more stable than the π-bonded one, for all complexes modeled, except the complex with the highest hydrogen loading, C_2H_4/H_7Rh_3.

To determine the adsorbate that is thermodynamically most favorable, we use Gibbs free energies of the structures examined. Figure 4A shows ΔG values of all intermediates adsorbed on supported Rh_3 clusters with respect to the total number of H, k, at 300 K. Ethylidyne is the most favorable intermediate on a Rh_3 cluster, for any hydrogen coverage studied. Other intermediates with ΔG values similar to that of ethylidyne were only found for systems with k = 7: ethylidene, CH_3CH/H_3Rh_3 as well as di-σ- and π-bonded ethene, di-σ-C_2H_4/H_3Rh_3 and π-C_2H_4/H_3Rh_3 which are less stable by 11 kJ/mol, 14 kJ/mol, and 23 kJ/mol, respectively.

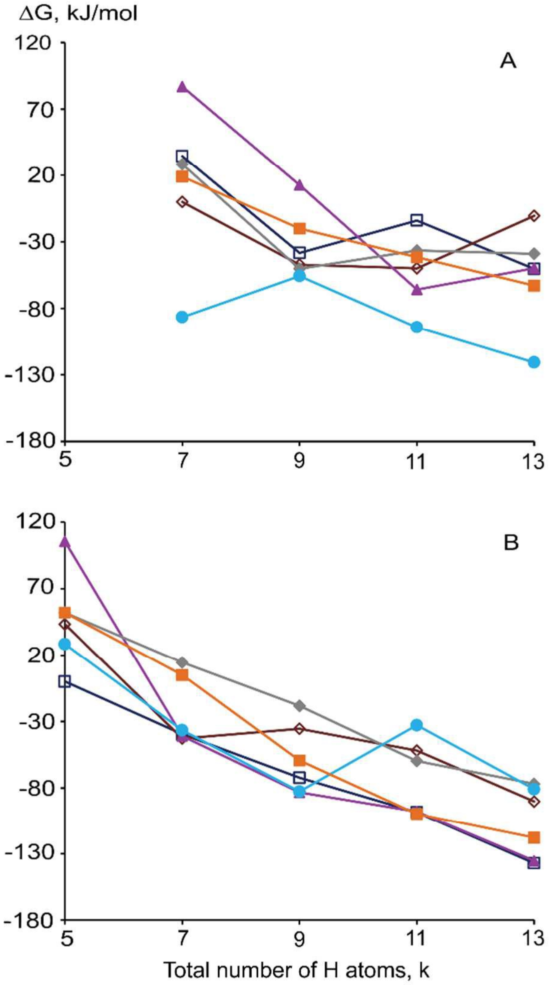

Figure 4. Change in the relative Gibbs free energies (300 K), ΔG, for modeled complexes of (A) Rh_3 and (B) Rh_4 clusters with increasing total numbers k of H atoms adsorbed. π-bonded ethene – empty blue squares, di-σ-bonded ethene – empty brown rhombs, ethyl (or pseudo ethyl) – magenta triangles, ethylidyne – cyan circles, ethylidene – filled orange squares, vinyl – filled grey rhombs. The vinylidene species are omitted in these graphs.

***Rh_4*.** Different from the ethene complexes of Rh_3, at Rh_4 the π-bonded configuration is more stable. The only exception is the structure with k = 7, C_2H_4/H_3Rh_4, where the difference in ΔE values is only 6 kJ/mol in favor of the di-σ species. For systems with k = 5, the most stable complex is π-C_2H_4/HRh_4. With increasing H loading of Rh_4, the order of stability changes in favor of the pseudo η-ethyl intermediate which is the most stable one for k = 7, 9, and 11 (Table 2). For the complexes with the highest hydrogen loading, k = 13, the structures π-C_2H_4/H_9Rh_4 and η-C_2H_5/H_8Rh_4 have essentially the same stability.

Figure 4B provides the ΔG values of $C_2H_x/H_{k-x}Rh_4$ complexes for the total number k of H atoms; the data for vinylidene are not included as these complexes are notably higher in energy, by more than 40 kJ/mol, than the most stable species. The tendency for the complexes on Rh_4 is not as clear as for the complexes on Rh_3. For k = 5 the most stable species is π-C_2H_4/HRh_4, but with more than 5 H atoms in the complex, two or more intermediates are thermodynamically favored; their ΔG values differ at most by 3 kJ/mol. For k = 7 the three most stable intermediates are pseudo η-ethyl, π- and di-σ-bonded ethene. For k = 9, the pseudo η-ethyl intermediate and ethylidyne are most stable. For k = 11, the most stable complexes are those of vinyl, pseudo η-ethyl, and π-C_2H_4; and for the highest hydrogen loading considered, k = 13, the two competing structures are π-C_2H_4/H_9Rh_4 and η-C_2H_5/H_6Rh_4. Thus, at variance with Rh_3 for which ethylidyne forms the most stable complexes at all hydrogen loadings modeled, the most favorable complexes involving Rh_4 mostly comprise π-bonded ethene and pseudo η-ethyl; but other species appear at specific hydrogen loadings.

The particular stability of ethylidyne on supported hydrogenated Rh_3 and Rh_4 clusters compared to other complexes may be connected to the influence of the organic species on the metal-metal bonding in the cluster. Ethylidyne binds to all three atoms of supported Rh_3 (Fig. S1 of ESI) and all three Rh-Rh distances are simultaneously elongated, with a maximum difference between shortest and longest distance of 8–18 pm for different values of k. The longest Rh-Rh distance, 276 pm, is calculated for clusters with the highest H loading, k = 9 and 11. On the other hand, ethylidyne coordinates to a triangle of the tetrahedral cluster Rh_4 and causes non-equivalent elongation of the Rh-Rh distances in that triangle. The maximum difference between the shortest and longest metal-metal distance is notably longer than in Rh_3, now 51–72 pm, because one of the Rh-Rh bonds breaks, with a distance of at least ~300 pm (Fig. S3 of ESI), and the cluster takes on a butterfly shape. Such bond cleavage likely is facilitated because each of the three Rh atoms binds to the fourth one. These bonds partially saturate the metal atoms, including those of the broken Rh-Rh bond, thus preserving the integrity of the metal moiety. The Rh-C and C-C distances are very similar in the ethylidyne complexes on both clusters, Rh_3 and Rh_4. Thus, the broken Rh-Rh bond decreases the stability of the ethylidyne complexes of Rh_4; in consequence, these structures exhibit a similar stability as those of the other intermediates, described above.

3.2.2. Thermodynamic model

Based on the calculated relative Gibbs free energies, we applied statistical mechanics to derive the partial equilibrium concentrations of the investigated organic intermediates at a given temperature and H_2 pressure; for the details of the procedure, see Section 1 of the ESI and Ref. 12. Figure 5 shows the distribution of partial concentrations of the dominant species among the complexes of Rh_3 and Rh_4 clusters for various temperatures at $P(H_2) = 10^4$ Pa. We selected this hydrogen pressure to represent the experimental findings of Gates et al.[4] at $P(H_2) = 10^4$ Pa where the Rh catalyst was highly selective for the hydrogenation of ethene. According to our results, in the case of Rh_3, the only intermediate favored at that hydrogen pressure is ethylidyne in the complex CH_3C/H_8Rh_3 with the highest hydrogen loading examined (Fig. 5A). For systems involving Rh_4 clusters, the complex of π-bonded ethene, π-C_2H_4/H_9Rh_4, is the most favored structure at temperatures below 300 K. With increasing temperature, the pseudo ethyl intermediate η-C_2H_5/H_8Rh_4 with highest value of H, k = 13, is formed to an appreciable amount, and the two species exist in competition (Fig. 5B). Thus, at a temperature of 303 K, as reported for the experiments,[4] our simulations suggest that both π-bonded ethene and pseudo ethyl intermediates are favored on a hydrogenated Rh_4 cluster, with a (relative) ratio of about 2 : 1.

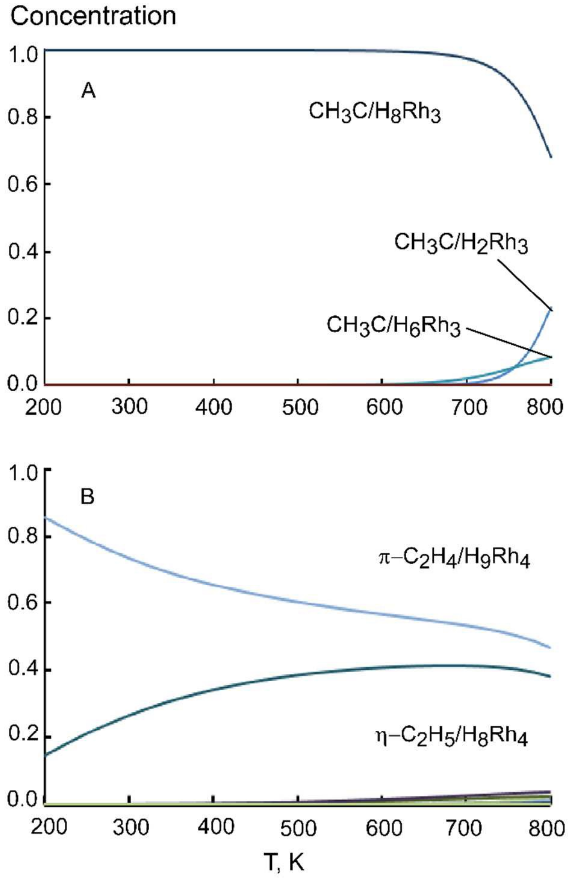

Figure 5. Molar fractions of the dominant species at $P(H_2)$ 10^4 Pa for different temperatures for complexes of (A) Rh_3 and (B) Rh_4 clusters.

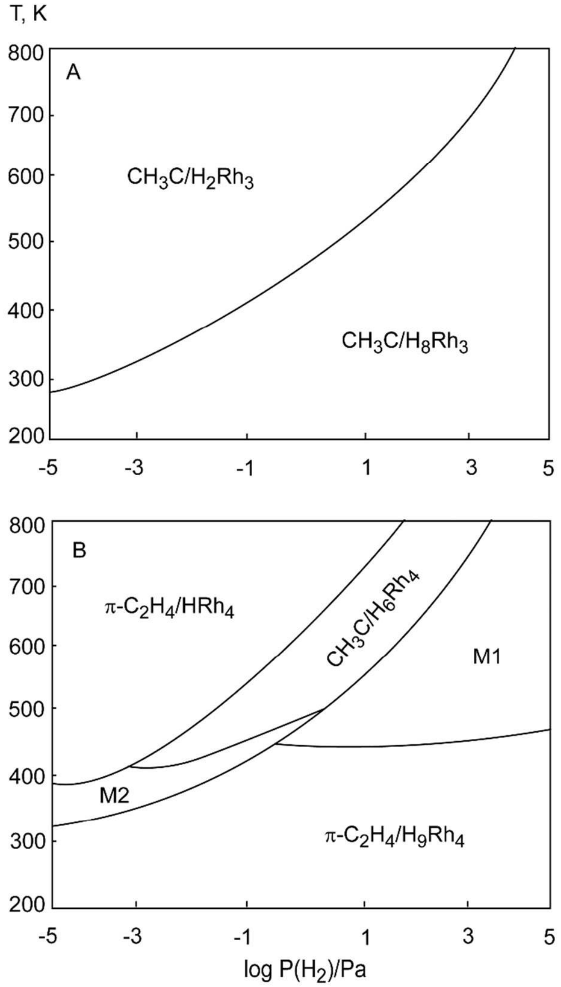

Figure 6. Phase diagram of dominant concentrations of intermediate complexes of (A) Rh_3 and (B) Rh_4 clusters as function of temperature T and hydrogen pressure $P(H_2)$. Species are considered as dominant when their concentration represents more than 2/3 of the total. If none of the species reaches that concentration, then the mixture of the two species with highest concentrations are reported. M1 denotes a mixture of π-C_2H_4/H_9Rh_4 and η-CH_3CH_2/H_8Rh_4, and M2 denotes a mixture of CH_3C/H_6Rh_4 and η-C_2H_5/H_4Rh_4.

To examine which species form preferentially at different hydrogen pressure, we constructed $P(H_2)$-T phase diagrams for both types of clusters, Rh_n (n = 3, 4) (Fig. 6). The resulting diagram for the complexes of the Rh_3 cluster (Fig. 6A) is quite simple: only ethylidyne appears as favorable species in the range of temperatures and $P(H_2)$ studied. In the complexes, only the amount k of H atoms in the system changes. At temperatures below 280 K, the highest hydrogen coverage, CH_3C/H_8Rh_3, is expected at any hydrogen pressure. The complex with low hydrogen content of the system, CH_3C/H_2Rh_3, may exist above 280 K at low hydrogen pressure, 10^{-5} Pa. With increasing pressure, this structure appears only at increasingly higher temperatures. The ethylidyne complexes with intermediate hydrogen loading of the metal moiety appear in very narrow intervals of pressure and temperature along the line in Figure 6A.

The phase diagram of the Rh_4 complexes involves more intermediates as two or more organic ligands of similar stability exist; see Subsection 3.2.1. At low hydrogen pressure and temperatures above 400 K, π-bonded ethene in the complex π-C_2H_4/HRh_4 is the dominant species with molar concentration above 2/3 of all species. In a certain intermediate range of (relatively high) temperatures, varying with H_2 pressure, ethylidyne, CH_3C/H_6Rh_4, is the dominant species (Fig. 6B). For lower temperatures, between 300 K and 500 K, and at very low P(H_2), below 1 Pa, ethylidyne and pseudo ethyl species, η-C_2H_5/H_4Rh_4, appear in similar concentrations (denoted as mixture M2 in Fig. 6B). At temperatures below 320 K, the dominant intermediate for any H_2 pressure is π-bonded ethene with highest amount of hydrogen atoms, π-C_2H_4/H_9Rh_4, adsorbed on the cluster. When the temperature reaches 440 K and H_2 pressure increase above 10^3 Pa (mixture M1 in Fig. 6B) π-bonded ethene competes with the pseudo ethyl structure η-CH_3CH_2/H_8Rh_4.

The phase diagrams in Fig. 6 clearly show the influence of the nuclearity of the metal cluster on the type of favored reaction intermediates. This finding may motivate further experimental analysis regarding the type of metal clusters that are appropriate for the catalytic hydrogenation of ethene. On the smaller cluster, Rh_3, the favored species is ethylidyne which is considered as spectator species that blocks the metal sites and thus prevents hydrogenation.[6, 30 - 34] Therefore, this type of rhodium cluster seems inappropriate for the catalytic hydrogenation of ethene. On the other hand, on a Rh_4 cluster, the pseudo ethyl intermediate appears among the dominant species in some regions of the phase diagram. As the formation of an ethyl-type intermediate and its subsequent hydrogenation to ethane is the preferred path of ethane formation,[13,14,35] According to the present computational results for model systems, Rh_4 clusters are suitable for the catalytic hydrogenation of ethene from thermodynamic point of view.

4. Conclusions

Using periodic density functional calculations we examined the structure and the stability of various ethene and ethene-derived intermediates that may appear during the hydrogenation of ethene on small zeolite-supported Rh_n clusters (n = 3, 4) with varying amounts of pre-adsorbed hydrogen on the metal moiety.

Although the two types of metal clusters considered in the present study differ by only one atom, their properties differ widely. For such drastic changes in the reactivity of metal clusters for varying nuclearity are well documented.[1,36] Regarding the structural properties, most of the intermediates studied show a similar coordination to both supported clusters studied, Rh_3 and Rh_4. An exception is the ethyl intermediate which is adsorbed in an on-top fashion to one center of Rh_3, whereas this coordination is not the most stable one in the complexes of Rh_4. For the latter complex, a structure, referred to as pseudo ethyl complex, was determined favorable that features two Rh-C contacts to the apical center of a Rh_4 tetrahedron and an additional bond of one of the H centers of the methyl moiety to the same Rh center. Similar coordination modes of CH_3CH_2 species to a metal moiety have been reported thus far only for transition state structures during the hydrogenation of π-bonded ethene to ethyl. Calculated rather low vibrational frequencies of C-H stretching modes (harmonic approximations in the range 2000–2500 cm^{-1}) involving the H center that interacts with a Rh center may offer a fingerprint for detecting this pseudo ethyl species because C-H frequencies of regular ethyl species are notably larger. The existence of such intermediates was not proposed so far, likely due to absence of metal atom with appropriate apical coordination as in the modeled supported tetrahedral Rh_4 cluster.

The main difference in the behavior of the Rh_3 and Rh_4 clusters is connected to the relative stability of the organic ligands modeled on the two supported clusters. The phase diagrams based on calculated Gibbs free energies, show different types of dominant species on the two clusters. On Rh_3, ethylidyne is the favored species over the whole range simulated for temperature and pressure; this dehydrogenation product of ethene is considered to be stable spectator species that blocks the metal sites. Therefore, such a rhodium cluster will not engage in the catalytic hydrogenation of ethene. In contrast, π-bonded ethene and the pseudo ethyl intermediate appear among the dominant species on highly hydrogenated Rh_4, at temperature above 440 K, thus at conditions close to those in experiment. In other words, in the models studied here, the catalytic hydrogenation of ethene to ethane seems feasible on Rh_4, but not on Rh_3. Although the zeolite-supported small rhodium clusters were used both in the experiments and computational modeling as prototypes of real rhodium-containing heterogeneous catalysts, our results suggest that the actual catalytic properties can be controlled by fine tuning of the size of the metal species.

Our conclusions may inspire new experimental studies of catalytic systems with precise control of the nuclearity of the supported metal cluster in the following two directions. First, the size-specific catalytic reactivity of very small supported rhodium clusters may be probed in ethene hydrogenation experiments. For this purpose, in a comparative study, preferentially Rh_3 and Rh_4 should be deposited on a well-defined support, e.g. on metal oxides[1,36,37] or open zeolite films.[38] Second, metal species with pseudo ethyl ligands, determined here to be a stable intermediate on Rh_4 clusters, may be identified by vibrational spectroscopy of small clusters containing an apical metal atom, using the low-frequency C-H mode as fingerprint.

Acknowledgments. VKM and GNV gratefully acknowledge funding by the FP7 project Beyond Everest. NR acknowledges a generous grant of computing resources by the Gauss Centre for Supercomputing (www.gauss-centre.eu), provided on the SuperMUC platform of Leibniz Supercomputing Centre Garching (www.lrz.de).

References

(1) U. Heiz, A. Sanchez, S. Abbet, W.-D. Schneider, *J. Am. Chem. Soc*., 1999, **121**, 3214–3217.

(2) B. C. Gates, *Top. Catal.,* 2001, **14**, 173–180.

(3) G. A. Somorjai, A. M. Contreras, M. Montano, R. M. Rioux, *Proc. Natl. Acad. Sci. U.S.A.,* 2006, **103**, 10577–10583.

(4) P. Serna, B. C. Gates, *J. Catal.,* 2013, **308**, 201–212.

(5) P. Serna, B. C. Gates, *J. Am. Chem. Soc.,* 2011, **133**, 4714–4717.

(6) A. M. Argo B. C. Gates, *J. Phys. Chem. B,* 2003, **107**, 5519–5528.

(7) H. J. Borg, R. M. Hardeveld, J. W. Niemantsverdriet, *J. Chem. Soc. Faraday Trans.,* 1995, **91**, 3679–3684.

(8) M. Li, W. Guo, R. Jiang, L. Zhao, X. Lu, H. Zhu, D. Fu, H. Shan, *J. Phys. Chem. C,* 2010, **114**, 8440–8448.

(9) D. L. S. Nieskens, A. P. van Bavel, D. Curulla Ferre, J. W. Niemantsverdriet, *J. Phys. Chem. B,* 2004, **108**, 14541–14548.

(10) D. Basaran, H. A. Aleksandrov, Z. Chen, Z. Zhao, N. Rösch, *J. Mol. Catal. A*: *Chemical,* 2011, **344**, 37–46.

(11) P. Raybaud, C. Chizallet, C. Mager-Maury, M. Digne, H. Toulhoat, P. Sautet, *J. Catal.*, 2013, **308**, 328–340.

(12) V. K. Markova, G. N. Vayssilov, N. Rösch, *J. Phys. Chem. C,* 2015, **119**, 1121–1129.

(13) Z. Zhao, L. V. Moskaleva, H. A. Aleksandrov, D. Basaran, N. Rösch, *J. Phys. Chem. C,* 2010, **114**, 12190–12201.

(14) L. V. Moskaleva Z. Chen, H. A. Aleksandrov, A. B. Mohammed, Q. Sun, N. Rösch, *J. Phys. Chem. C,* 2009, **113**, 2512–2520.

(15) G. P. Petrova, G. N. Vayssilov, N. Rösch, *Catal. Sci. Technol.* 2011, **1**, 958–970.

(16) G. N. Vayssilov, B. C. Gates, N. Rösch, *Angew. Chem., Int. Ed.,* 2003, **42**, 1391–1394.

(17) G. N. Vayssilov, N. Rösch, *J. Phys. Chem. B,* 2004, **108**, 180–197.

(18) G. Kresse, J. Furthmüller, *Comput. Mater. Sci.,* 1996, **6**, 15–50.

(19) G. Kresse, J. Furthmüller, *Phys. Rev. B,* 1996, **54**, 11169–11186.

(20) J. P. Perdew, K. Burke, M. Ernzerhof, *Phys. Rev. Lett.,* 1996, **77**, 3865–3868.

(21) P. E. Blöchl, *Phys. Rev. B,* 1994, **50**, 17953–17979.

(22) G. Kresse, D. Joubert, *Phys. Rev. B,* 1999, **59**, 1758-1775.

(23) S. Grimme, *J. Comp. Chem.,* 2006, **27**, 1787–1799.

(24) W. Tang, E. Sanville, G. Henkelman, *J. Phys.: Condens. Matter,* 2009, **21**, 084204–084207.

(25) P. W. Atkins, *Physical Chemistry*, 7th ed.; Oxford University Press, Oxford 2002.

(26) G. P. Petrova, G. N. Vayssilov, N. Rösch, *J. Phys. Chem. C,* 2008, **112**, 18572–18577.

(27) M. Neurock, R. A. van Santen, *J. Phys. Chem. B,* 2000, **104**, 11127–11145.

(28) P. St. Petkov, G. P. Petrova, G. N. Vayssilov, N. Rösch, *J. Phys. Chem. C,* 2010, **114**, 8500–8506.

(29) E. A. Owen, E. I. Yates, *Philos. Mag.,* 1933, **15**, 472–488.

(30) P. S. Cremer, X. Su, Y. R. Shen, G. A. Somorjai, *J. Am. Chem. Soc.,* 1996, **118**, 2942–2949.

(31) A. L. Marsh, G. A. Somorjai, *Top. Catal.* 2005, **34**, 121–128.

(32) P. S. Cremer, G. A. Somorjai, *J. Chem. Soc., Faraday Trans.* 1995, **91**, 3671–3677.

(33) A. M. Argo, B. C. Gates, *Langmuir* 2002, **18**, 2152–2157.

(34) G. N. Vayssilov, *Adv. Colloid Interface Sci.* 1993, **47**, 25–57.

(35) H. A. Aleksandrov, S. M. Kozlov, S. Schauermann, G. N. Vayssilov, K. M. Neyman, *Angew. Chemie Int. Ed.,* 2014, **53**, 13371–13375.

(36) U. Heiz, U. Landman, (Eds.). *Nanocatalysis*, Springer, Berlin 2007.

(37) U. Heiz, E. L. Bullock, *J. Mater. Chem.,* 2004, **14**, 564-577.

(38) S. Shaikhutdinov, H. J. Freund, *Adv. Mater.,* 2013, **25**, 49–67.

TOC entry

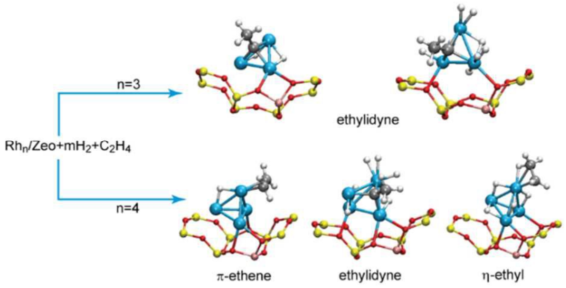

Phase diagrams from DFT modeling suggest that zeolite-supported Rh_4 clusters may be appropriate for the catalytic hydrogenation of ethene to ethane, whereas Rh_3 clusters favor the formation of stable adsorbed ethylidyne species, preventing further hydrogenation.